Polymer-induced orientation of nanowires under electric fields

Paloma Arenas-Guerrero[a], Ángel V. Delgado[a], Silvia Ahualli[a], María L. Jiménez*[a]

[a]*Department of Applied Physics, University of Granada, Avda. de Fuente Nueva sn, 18071, Granada, Spain*

Abstract

The controlled orientation of metallic wires inside a polymeric medium can enhance desired properties of the composites, such as the electrical conductivity or the optical transmittance. In this work, we study silver nanowire orientation in semidilute suspensions of DNA and find an intriguing effect: under the application of low-frequency AC electric fields with moderate amplitude, the DNA coils can provoke the orientation of the wires in solution. The phenomenon is entirely induced by the polymer, when it is deformed by the application of an electric field. This effect is explained using computer simulations based on excluded-volume interactions. Moreover, we experimentally show that such a behaviour is not exclusive of silver nanowire-DNA suspensions, but rather occurs for other particle-polymer systems. This phenomenon can be taken advantage of to achieve strong orientation of particles otherwise insensitive to electric fields.

Keywords: Silver nanowires, DNA, nanoparticle alignment, particle-polymer interactions

1. Introduction

Nanoparticle-polymer composites present high prospects for many applications related to synergistic phenomena emerging in these systems. As examples, we can mention their use in the fabrication of mechanically reinforced materi-

*Corresponding author, Tel: +34 958 24 27 43, E-mail: jimenezo@ugr.es

Email addresses: palomaag@ugr.es (Paloma Arenas-Guerrero), adelgado@ugr.es (Ángel V. Delgado), sahualli@ugr.es (Silvia Ahualli)

als, biocompatible ferrogels for tissue engineering, tunable metamaterials, plasmonic displays, hydrogels for drug delivery or catalytic membranes [1–6]. Often, the controlled orientation of non-spherical nanoparticles inside the polymeric matrix greatly enhances the desired properties. For instance, upon particle alignment, improved energy storage capacity, catalytic properties, thermal conductivity or mechanical performance have been observed for different particle-polymer nanocomposites [7–12].

Several techniques are available for the orientation of non-spherical nanoparticles, including the Langmuir-Blodgett method, microfluidics, electrospinning, jet printing, brush coating or spray-assisted alignment [13–19]. Direct in-situ growth of oriented nanorods in polymer fibers has also been reported [20]. Another possibility is the use of templates, such as those based on carbon nanotubes or liquid crystalline phases of cellulose nanocrystals [21, 22]. The direct application of electromagnetic fields to particle suspensions is also an attractive option [23–27]. Each of these techniques presents its own limitations, which can be further increased by the presence of a polymer. For instance, viscous forces have been shown to hinder the orientation of carbon nanotubes inside a polymeric matrix [28].

As examples of aligned elongated particles, we can mention semiconducting zinc oxide nanorods, which are used i.e. for the fabrication of perovskite solar cells [29, 30]. Oriented quantum rods have also gathered attention due to their applications in liquid crystal displays [31, 32]. Moreover, considerable interest has been devoted to metallic nanorods, which have been oriented by solvent-evaporation or electrodeposition [33–36], in addition to direct application of electric fields [37–40]. The alignment of silver nanorods due to optical torques caused by the application of a polarised laser beam has also been theoretically studied [41].

In our case, we focus on aligned silver nanowires (Agnws), which also present a wide range of applications. For example, Agnw-polymer composites are used in the fabrication of conductive membranes to obtain transparent flexible electrodes [42–45]. In these systems, the alignment of the silver nanowires can enhance both the electrical conductivity and the optical transmittance, thus improving the performance of optoelectronic devices such as polymer light-emitting diodes or solar cells [46–48]. Furthermore, silver nanowires present antibacterial properties, making these electrodes suitable for biomedical applications [49]. For biocompatibility, DNA has been suggested as a suitable polymeric matrix for electrode fabrication [50, 51].

In this work we show that, under the application of low-frequency electric

fields, DNA can induce the orientation of silver nanowires in solution. Interestingly, moderate field amplitudes (around 8 V/mm for 1 Hz fields) are sufficient to align the Agnws almost completely in a semidilute DNA suspension via this phenomenon. The alignment is entirely caused by the DNA, and does not occur in its absence. It is, to our knowledge, the first time that particle alignment induced by a semidilute polymer suspension has been reported. Other approaches for polymer-mediated particle orientation are based either on polymer structures or a liquid crystalline phase [22, 52–54].

2. Experimental section

2.1. Materials

The silver nanowires used in this work were purchased from PlasmaChem, Germany (PL-AgW50). Fig. 1a shows a transmission electron microscopy picture of the particles. More images can be found in the Supplementary Information (SI) file. We determined a nanowire diameter of 45 ± 10 nm, within the range given by the manufacturer. The proportion of irregular and spherical silver particles is below 8%, as deduced from the observation of 175 particles.

On the other hand, the length of the Agnws shows a more significant polydispersity, as can be observed in Fig. 1b, which displays the length distribution (in volume) of the nanowires. This histogram was obtained via electric birefringence measurements, following the multi-exponential method, which has been proven useful for the size characterisation of polydisperse non-spherical particles [55]. The mean length (number-averaged) of the distribution is 1.8 μm.

The particle composition has been studied by energy dispersive X-ray analysis (Fig. 2). As observed, the wire core is made of silver. The nitrogen signal indicates the presence of a thin coating of polyvinylpyrrolidone ($(C_6H_9NO)_n$), which provides a small negative charge, stabilising the particles [56]. In a 1 mM NaCl electrolyte, the zeta potential of the coated particles is -19 mV (Malvern Zetasizer NanoZS, Malvern Instruments, UK).

The sepiolite needles were purchased from Merck. In a 1 mM NaCl electrolyte, they present a zeta potential of -25mV. A microscopy picture of these particles is provided in the SI file. Calf thymus and salmon testes DNA was purchased from Merck, Germany (D1501 and D1626, respectively). Poly(ethylene oxide) of two molecular weights, 35k and 4M, was also purchased from Merck (Germany). Poly(acrylic acid) (Carbopol 981, lightly cross-linked) was obtained from Lubrizol (USA).

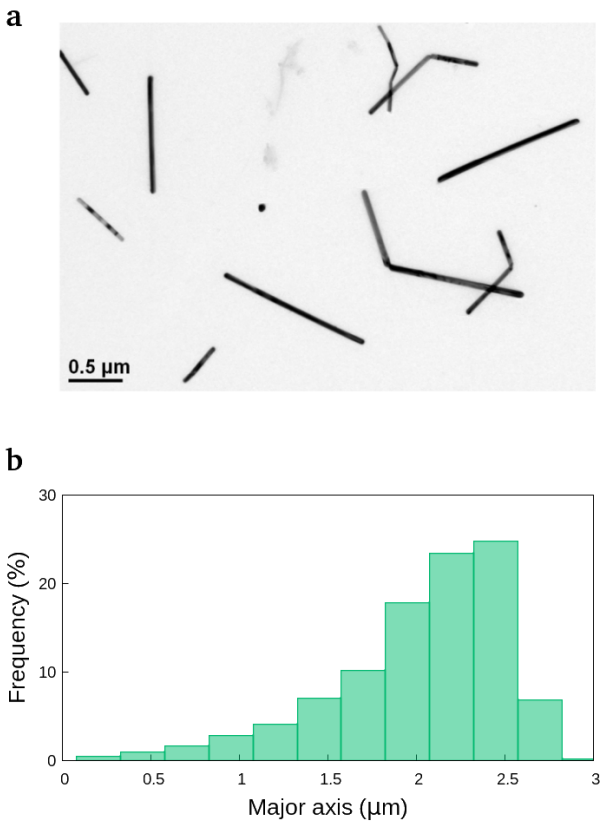

Figure 1: (a) High-resolution electron transmission microscopy image of the silver nanowires. (b) Length histogram of the Agnws, in volume, obtained via the analysis of the electric birefringence using the multi-exponential method.

All the polymers and the particles used in this work present a negative or neutral charge. This avoids any electrostatic attraction between the particles and the polymer in the bidisperse systems. The medium conductivity is 126 μS/cm in all samples, which corresponds to a 1 mM NaCl electrolyte. More information on sample preparation can be consulted in the SI file.

2.2. Methods

The device used for the determination of particle orientation, detailed elsewhere [39], is based on the measurement of the electric birefringence of the samples. Briefly, a He-Ne laser beam traverses a polariser, the Kerr cell, a quarter-wave plate and another polariser, reaching a photodiode. The Kerr cell contains

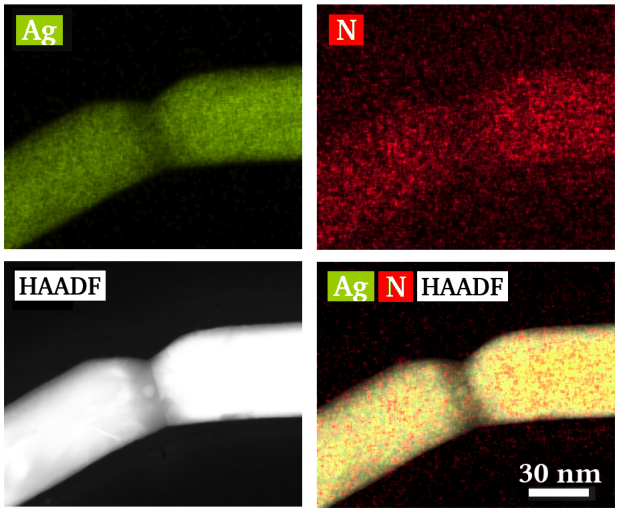

Figure 2: Energy dispersive X-ray analysis of two Agnws touching at the tips: silver mapping (top left), nitrogen mapping (top right), high-angle annular dark field image (bottom left) and combination of the three signals (bottom right).

the sample, in which stainless steel electrodes are immersed. When an alternating electric field is applied to the suspension, particle orientation makes the sample anisotropic and, hence, birefringent. This modifies the light transmitted by the setup. More information on the experimental device can be consulted in the SI file.

The electric birefringence is a very suitable technique for the measurement of particle alignment, since it can detect even very weak orientations. It also offers very good statistics, as a huge number of particles are evaluated at the same time. The experiments were repeated several times in order to check that the samples do not undergo any irreversible process, such as DNA degradation or particle aggregation.

3. Results and discussion

3.1. The DNA-induced Agnw orientation: experimental results

The average orientation of elongated particles can be described via the orientational order parameter of the system, defined as

$$S = \frac{1}{2}\langle 3\cos^2\theta - 1\rangle \tag{1}$$

being θ the angle between the field that produces the orientation and the symmetry axis of the particle. This parameter has a value of $S = 0, 1$ for randomly oriented and perfectly aligned systems, respectively. Here, we study the orientation of silver nanowires in a calf thymus DNA (CT-DNA) suspension under the application of an AC electric field.

When non-spherical particles are oriented due to the application of an electric field, the refractive index n of the sample becomes anisotropic. In this situation, we can define the electric birefringence of the suspension as $\Delta n = n_{\parallel} - n_{\perp}$, where the subscripts refer to the directions parallel and perpendicular to the applied field. The electric birefringence relates to particle orientation as [57]:

$$\Delta n = \Delta n_{\text{sat}} S \tag{2}$$

where Δn_{sat} is the saturation birefringence, that is, the value of Δn when particles are perfectly aligned (S=1). Therefore, we can determine particle electro-orientation by measuring the electric birefringence of the suspension. The value of Δn_{sat} has been experimentally obtained, as it is presented in the SI file.

Fig. 3 displays the experimental orientational order parameter of the Agnws in two DNA solutions, as a function of the frequency of the applied electric field. For comparison purposes, the order parameter of the Agnws in the absence of DNA is also included in the same graph. This spectrum is qualitatively similar to the ones presented elsewhere [39, 58] for silver nanowires in aqueous suspension. The only difference is that, in those works, some orientation due to induced-charge electro-osmosic flows was observed at low and medium frequencies. In our case, the ionic concentration is much higher (1 mM NaCl), and such an effect is negligible.

In order to describe the curves in Fig. 3, we consider three different ranges. For high frequencies ($\sim$100 kHz-10 MHz), the Agnws are substantially oriented both in the presence and absence of DNA. This behaviour is due to the so-called electro-orientation of the metallic wires, depicted in Fig. 4a. In this frequency regime, silver particles have been shown to undergo a strong polarisation due to charge separation inside the wire. This causes an induced dipole, and hence a torque, that aligns the particle along the field direction [39, 58].

In the medium-frequency range ($\sim$100 Hz-100kHz), the ions in solution have time to move and accumulate near the silver nanowires, screening their induced dipole (Fig. 4b). This reduces particle alignment to a nearly null value, as already observed elsewhere [39, 58]. Both in the high- and medium-frequency ranges, the value of S_{Agnws} is practically identical in the absence and presence of DNA, that is, the DNA coils do not affect the particle behaviour.

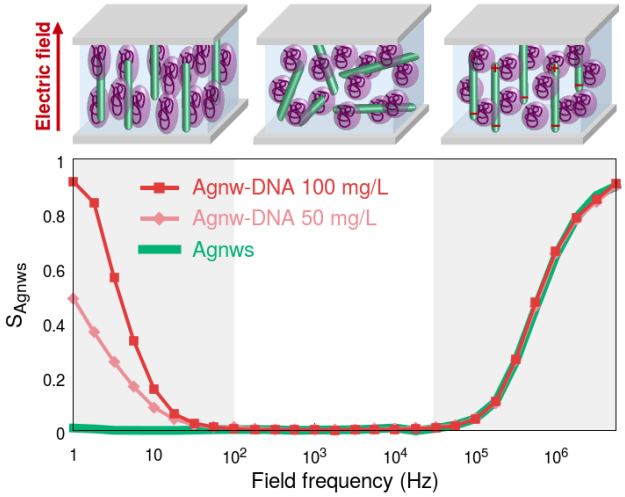

Figure 3: Spectrum of the orientational order parameter of the Agnws in a 100 mg/L (dark red square points) and a 50 mg/L (light red diamond points) DNA suspension. The Agnw concentration is 100 mg/L and the field strength is 8 V/mm. For comparison, the spectrum of a 100 mg/L Agnw suspension (green solid line) is also shown. A schematic representation of the Agnw-DNA system in the low-, medium- and high-frequency ranges is displayed above the graph, and further explained along the text.

For low field frequencies (1-100 Hz), the Agnws still exhibit no overall polarisation (Fig. 4c). For this reason, no orientation is observed in the case of the Agnw suspension. Nevertheless, in the Agnw-DNA system, the metallic particles undergo a strong alignment, comparable to that in the high-frequency range. This effect (the anomalous low-frequency orientation, hereafter) is observed solely in the presence of DNA, and hence it must be related to the interplay between the silver particles and the DNA coils. Moreover, these interactions must occur only at low frequencies.

Next, we show that the anomalous orientation of the Agnws below 100 Hz is significantly correlated to the stretching of the DNA coils. For this purpose, we study the electric birefringence of a DNA sample: when an electric field is applied to a DNA suspension, an induced dipole appears on the chain segments of the macromolecules, causing their orientation. This results in extended conformations of the chains, that is, in a deformation of the DNA coils [59]. Images of the deformation of the DNA coils have been obtained in several works, using different microscopy techniques (mainly fluorescence and atomic force microscopy), although in these experiments the macromolecule is placed near a surface [60–63].

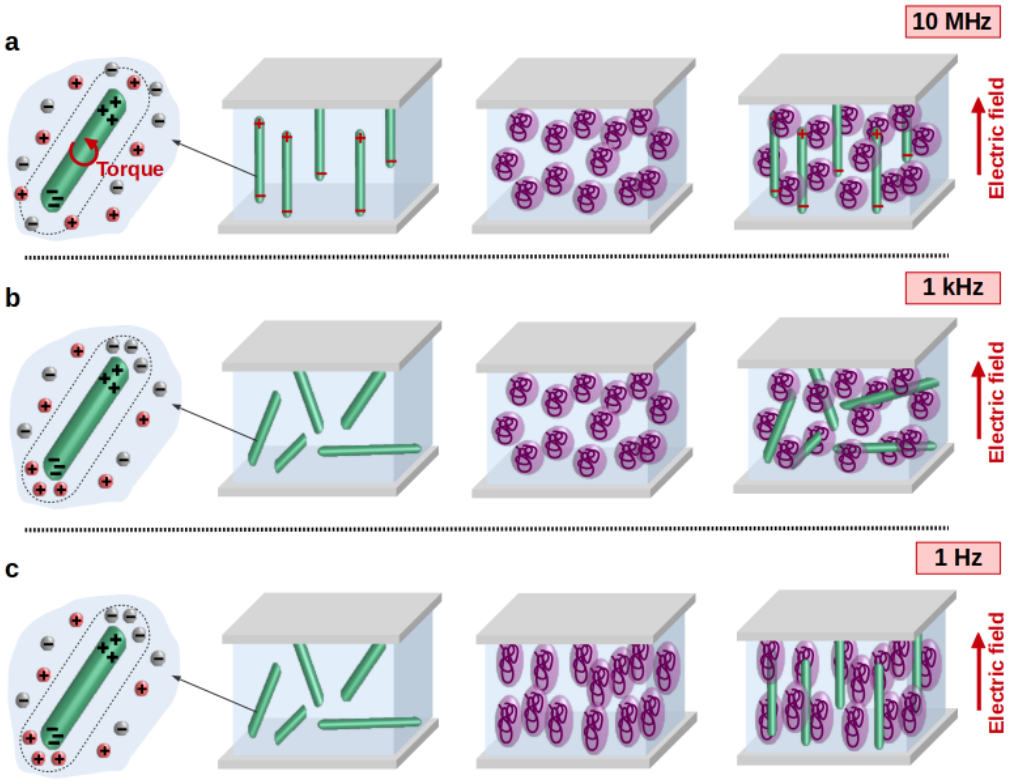

Figure 4: Schematic representations of the studied systems under the application of a vertical AC electric field of (a) 10 MHz, (b) 1 kHz and (c) 1 Hz. The first column shows the polarisation of a silver nanowire in a NaCl suspension. The red spheres represent Na^+ ions, whereas the grey ones are the Cl^- ions. The second, third and fourth columns depict an Agnw, DNA and Agnw-DNA suspension under the application of the aforementioned electric fields.

The stretching of DNA coils in suspension upon application of an electric field gives rise to an overall optical anisotropy of the sample, that is, a birefringence signal [59, 64]. This birefringence is directly related to the degree of deformation of the DNA coils. Hence, measuring the electric birefringence of DNA allows us to study the stretching of the macromolecule under the applied fields.

Fig. 5 shows the birefringence spectrum of a 1 g/L DNA suspension in a 1 mM NaCl electrolyte. The negative sign of the DNA birefringence was expected, and is due to base orientation inside the chains [64, 65]. Moreover, it must be noted that the DNA birefringence is negligible as compared to that of the Agnws. In our experiments, it is always ensured that $\Delta n_{\mathrm{DNA}} < 0.02\Delta n_{\mathrm{Agnws}}$. Hence, the

DNA signal can be neglected when studying Agnw-DNA suspensions. The results found for the birefringence spectrum of DNA are very similar to those reported elsewhere [59].

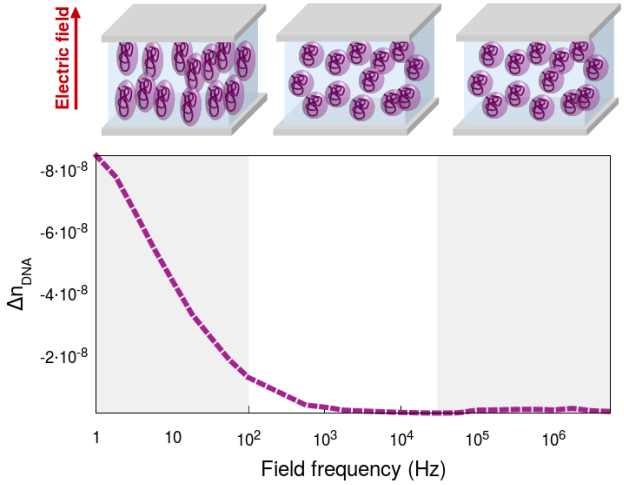

Figure 5: Spectrum of the electric birefringence of a 1 g/L DNA suspension in a 1 mM NaCl electrolyte. The field amplitude is 8 V/mm. A schematic representation of the system in the low-, medium- and high-frequency ranges is displayed above the graph, and further discussed along the text.

In order to analyse Fig. 5, we consider again different ranges. For medium and high frequencies, the DNA response is negligible. Inside these regimes, the effect of the DNA on the Agnw orientation is null, as already discussed (Figs. 3, 4a and 4b). On the other hand, below 100 Hz, the DNA exhibits a birefringence signal, which indicates the stretching of the DNA depicted in Fig. 4c. The DNA birefringence rapidly grows as the field frequency lowers, a dependence which is clearly similar to that of S_{Agnws} in the Agnw-DNA systems (low-frequency range in Fig. 3). From these data, it can be inferred that the alignment of the Agnws in the presence of DNA is associated with the response of the macromolecule to the external electric field, which occurs only in the low frequency regime.

The correlation between the low frequency DNA elongation and the orientation of the Agnws is reinforced by the experimental data in Fig. 6. Here, we show the alignment of the Agnws in DNA suspension as a function of the DNA concentration (c_{DNA}), for different values of the field frequency. As observed, for 1 kHz, 100 kHz and 1 MHz, the orientation of the Agnws in the Agnw-DNA suspension is independent of DNA concentration. This is in agreement with the finding that,

for medium and high frequencies, the DNA does not affect the Agnw orientation. On the other hand, for the 10 Hz field, the Agnw alignment grows with c_{DNA}. This behaviour was expected, since we concluded that, in the low-frequency range, the Agnw orientation is induced by the deformation of the DNA coils. This occurs only for frequencies below 100 Hz, where the dependence with the DNA concentration is indeed observed.

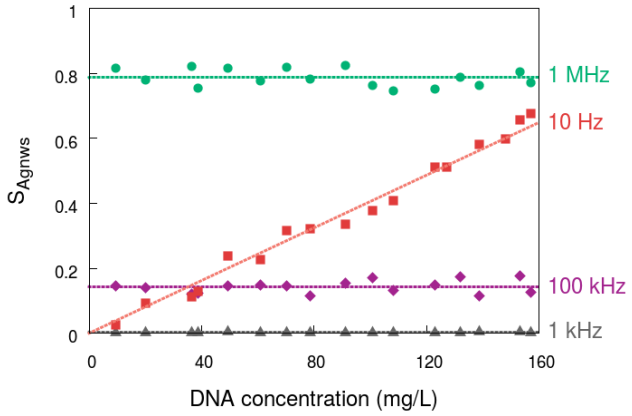

Figure 6: Orientational order parameter of the Agnws in a DNA suspension as a function of DNA concentration. The field strength is 8 V/mm and the Agnw content 100 mg/L. The points are the experimental data. The horizontal dotted lines represent the average S_{Agnws} value for 1 MHz, 100 kHz and 1 kHz. The red dotted line is a linear fitting of the 10 Hz data.

In light of these results, we can affirm that DNA deformation under the application of a low-frequency electric field can induce a strong alignment on the suspended Agnws. Elsewhere, the orientation of polymer chains by strong magnetic fields has been shown to cooperate with the alignment of embedded carbon nanotubes, which also interact with the field [52]. Moreover, the mechanical stretching of a polymer film can induce the orientation of gold nanorods or carbon nanotubes inside it [53, 66]. It has also been shown that gold nanorods immersed in a lyotropic DNA liquid crystal can be aligned by the application of mechanical shear [54]. However, in our case, we do not work with a polymer structure or a liquid crystalline phase, but rather with semidilute polymer solutions which behave as newtonian fluids. It is, to our knowledge, the first time that strong particle orientation due to a fully polymer-induced mechanism has been reported for such low concentrations. Moreover, in our case we use moderate electric fields to achieve the particle alignment, and not mechanical forces or strong magnetic fields.

More information can be extracted from the dynamic behaviour of the Agnw orientation, which is analysed in the SI file. Interestingly, the orientation time is visibly different for low (1.03 s) and high frequencies (1.85 s). This further supports the existence of different orientation mechanisms in these two regimes. The effect of the Agnw concentration is also presented in the SI document. We found that S_{Agnws} is independent of particle concentration, which rules out any interaction amongst the silver nanowires [39]. The orientation of the Agnws in a DNA suspension has also been studied via microscopy observations (see SI file). Moreover, in the SI document, further data on the birefringence of DNA are presented, including measurements for different concentrations and molecular weights.

3.2. The underlying mechanism of polymer-induced orientation

The DNA-induced low-frequency orientation of the Agnws, presented above, indicates that there must exist an interplay between the DNA and the silver nanowires. Here, we propose that this interaction is related to excluded-volume effects: when the DNA coils are stretched by a low-frequency electric field, the volume available for the Agnws becomes anisotropic, favouring the alignment of the nanoparticles. In this case, the mechanism should not be exclusive of DNA, but rather we expect other macromolecules to exhibit a similar behaviour.

In Fig. 7a we analyse the order parameter of the Agnws in two different suspensions of poly(ethylene oxide) (PEO). We use short and long PEO chains, with an average molecular weight of 35 kDa (PEO 35k) and 4 MDa (PEO 4M) respectively. This corresponds approximately to a contour length of L_c=280 nm and L_c=32 μm. In this Figure, it can be observed that the anomalous low-frequency effect is also present in these systems, showing that the polymer-induced orientation is not exclusive of DNA. Moreover, we find that, for the same polymer, longer chains give rise to a more pronounced anomalous effect.

This is further supported by the data in Fig. 7b, which shows the results obtained for different Agnw-DNA suspensions. Here, it can be observed that the already used calf thymus DNA (CT-DNA, $\sim$15 kbp, L_c=5.1 μm [67]) induces a larger Agnw orientation than shorter salmon testes DNA chains (ST-DNA, $\sim$2 kbp, L_c=0.68 μm [68]). From these data, we can conclude that the polymer-induced Agnw orientation is enhanced with L_c. This behaviour was expected, since the radius of gyration grows with the contour length [69], and hence longer polymers are associated to larger excluded volumes.

Despite this, it must be noted that the Agnw-PEO 4M system exhibits a very small anomalous effect as compared to both types of DNA. Indeed, even though

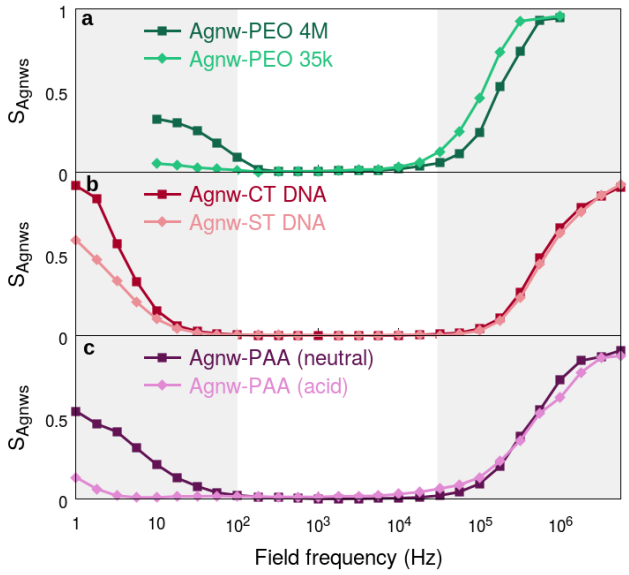

Figure 7: Spectra of the orientational order parameter of the Agnws in suspension with different polymers: (a) Agnws and PEO with the indicated molecular weights; (b) Agnws and calf thymus or salmon testes DNA; (c) Agnws and PAA in acid or neutral pH conditions. In the case of Agnw-PEO, polymer concentration is 500 mg/L and the field strength 20 V/mm. For the Agnw-DNA and Agnw-PAA systems, polymer concentration is 100 mg/L and the field strength is 8 V/mm. The Agnw concentration is always 100 mg/L.

PEO 4M is the longest polymer used in this work, in order to observe the low-frequency orientation it was necessary to use an electric field 2.5 times more intense and a suspension five times more concentrated than in the case of DNA. This shows that the analysis of the contour length is not sufficient to characterise the behaviour. Instead, the persistence length, L_p, also seems to play an important role.

To study such a dependence, we use poly(acrylic acid), hereafter referred to as PAA. This polymer has been prepared in two different manners. First, we use it with its natural (acid) pH, under which it assumes a partially coiled configuration due to strong hydrogen bonding. Secondly, we set the pH to a higher (close to neutral) value. Under this condition, the PAA chain acquires a negative charge, and electrostatic repulsion increases the persistence length, favouring the uncoiling of the polymer [70]. The results are shown in Fig. 7c, where it can be observed that the anomalous low-frequency effect is considerably larger for the PAA with neutral pH.

In light of these results, it can be concluded that the persistence length has a critical impact on the low-frequency Agnw orientation, which is greatly enhanced for stiffer polymers. For this reason, DNA provides the best results, since this macromolecule is known to exhibit a particularly large value of the persistence length. This behaviour is in agreement with our hypothesis based on excluded-volume interactions, since an increase in L_p translates into a larger radius of gyration of the polymer [69], and hence a larger excluded volume.

Lastly, it must be noted that, according to our hypothesis of anisotropic excluded-volume interactions, the polymer-induced orientation should occur not only for the Agnws, but also for other particles with a similar geometry. In order to check this, we studied sepiolite-DNA suspensions. The experimental data are shown in the SI file. We found that the anomalous effect is indeed present also in this system, so it is not exclusive of the metallic wires. These results show that the low-frequency polymer-induced orientation is a phenomenon common to different systems of a polymer and elongated particles.

3.3. Simulation of the polymer-induced Agnw orientation

In order to further understand the DNA-induced orientation of the Agnws under low frequency AC electric fields, we have performed a simulation of the Agnw-DNA systems. For the interplay between the polymer and the particles, we consider only anisotropic excluded-volume interactions, since we propose that this is the underlying mechanism giving rise to the anomalous effect.

For the modelling of the polymer, we consider a freely jointed chain of N_K Kuhn segments of length $L_K = 2L_p$ [69]. The used value of the persistence length is 65 nm, reported for DNA in a 1 mM NaCl electrolyte [71]. The number of Kuhn segments is given by the contour length ($N_K = L_c/L_K$). In the absence of a low-frequency electric field, we perform an isotropic random walk of the Kuhn segments, and calculate their root mean square distance to the center of mass of the polymer, that is, the radius of gyration. For the simulation, the polymer coils are substituted by spheres with this radius.

On the other hand, in order to study the polymer in the presence of a low-frequency electric field, the coils must be modelled as spheroids instead of spheres. To obtain the spheroid dimensions, we again study the macromolecule as a freely jointed chain. However, in this case we perform a walk with a preferential orientation along the field direction. For this purpose, we choose a continuous angular probability distribution of the Kuhn segments, with a tunable maximum in the direction of the electric field. A more pronounced probability peak results in more oriented Kuhn segments and hence a more elongated coil.

The equivalent spheroid semiaxes, a and b, are obtained by calculating the root mean square distance of the Kuhn segments to the center of mass, in the directions parallel and perpendicular to the external field respectively. These dimensions are related to the average order parameter of the Kuhn segments, S_K, defined as given by Eq. 1. Such orientation can be tuned by modifying the probability distribution of the anisotropic walk of the Kuhn segments. Hence, the degree of stretching of the DNA coils can be empirically taken into account in our simulation. More details on the modelling of the polymer coils can be consulted in the SI file.

In the next step, we randomly place the equivalent spheres or spheroids in a unit volume, allowing some overlap. In order to do so, we use the intercoil potential provided elsewhere [72]. When placing the spheroids, their longest dimension must be always kept along the field direction. The number of polymers per unit volume is calculated from the experimental DNA concentration value. Lastly, the Agnws are modelled as infinitely thin wires with a length of 1.8 μm.

As explained, in our simulation the presence of the low-frequency electric field is mimicked by a tunable elongation of the DNA coils, with no direct effect on the Agnws. This is based on the experimental finding that, for low frequencies, electric fields do not cause any orientation of the silver wires in the monodisperse suspension (see Agnws in Fig. 3). Nonetheless, in the bidisperse system, the silver nanowires are constrained by the presence of the elongated DNA coils: in the simulation, we place an Agnw in the DNA suspension, and only if the position yields no overlap with the spheroids, it is allowed. The process is iterated until 5,000 permitted positions have been studied. The orientational order parameter of the silver nanowires (Eq. 1) is obtained as the average value of all allowed configurations. Further details on the simulation procedure can be found in the SI document.

Fig. 8 displays images of the simulated system in different conditions. A portion of 3x3x3 μm^3 of the system is shown. The purple spheroids are the DNA coils inside this region (there are more coils on the border, but they have been removed from the image to facilitate the visualization). The green segments represent 100 allowed positions of a single Agnw. That is, these lines are not different Agnws, but possible positions of one particle. This is important, since the Agnw concentration is very small (1 Agnw in 7x7x7 μm^3 for an Agnw concentration of 100 mg/L, see SI file).

In Fig. 8a, it can be observed that, for the more concentrated sample, the Agnw is more constrained and therefore more aligned. Fig. 8b shows that, when no electric field is applied (spherical coils), the excluded volume, and hence the Agnw orientation, are isotropic. In contrast, when the DNA coils are deformed due to

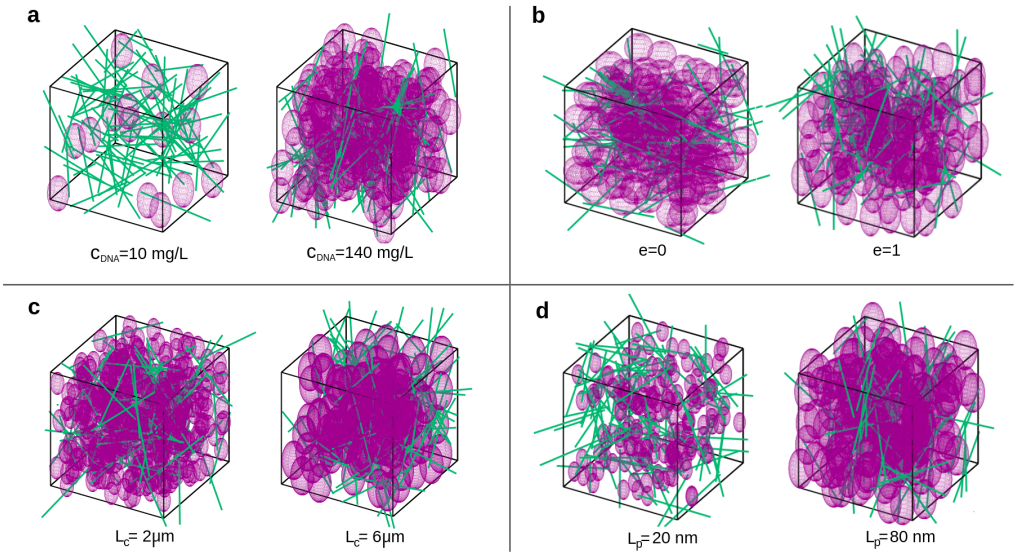

Figure 8: Representation of the Agnw-DNA system for different values of (a) the concentration, (b) the elongation, (c) the contour length, and (d) the persistence length of the DNA, as provided by our simulation. Unless indicated otherwise, c_{DNA}=100 mg/L, e=0.8, L_c=5.1 μm and L_p=65 nm. The purple spheroids are the DNA coils and the green segments represent 100 allowed positions of a single Agnw. The side of the cube is 3 μm.

the application of an AC electric field, the Agnw presents a preferential orientation along the field direction. Lastly, in Figs. 8c and 8d it can be observed that, when L_c or L_p are increased, the excluded volume grows and the Agnws are more aligned.

Fig. 9a shows the value of S_{Agnws} as a function of DNA concentration, as calculated by our simulation. In this computation, the DNA elongation ($e = \frac{a}{b} - 1$) presents a value of e=0.8. For comparison, we also include the experimental results from Fig. 6 at 10 Hz. As observed, the simulation correctly predicts the linear dependence of the Agnw orientation as a function of c_{DNA}, below the overlap concentration ($\sim$110 mg/L). This qualitative agreement shows that the simulation, although somewhat limited, is able to capture the essential features of the low-frequency effect in particle-polymer suspensions. Quantitative agreement can also be considered satisfactory for the chosen value of the elongation. Since the excluded volume is proportional to the DNA concentration, in light of these results we can write, as an approximation, $S_{\mathrm{Agnws}} \propto c_{\mathrm{DNA}} \propto V_{\mathrm{ex}}$. This dependence is reasonable taking into account that the basis of our model is that the orientation

of the Agnws is due to anisotropic excluded-volume effects.

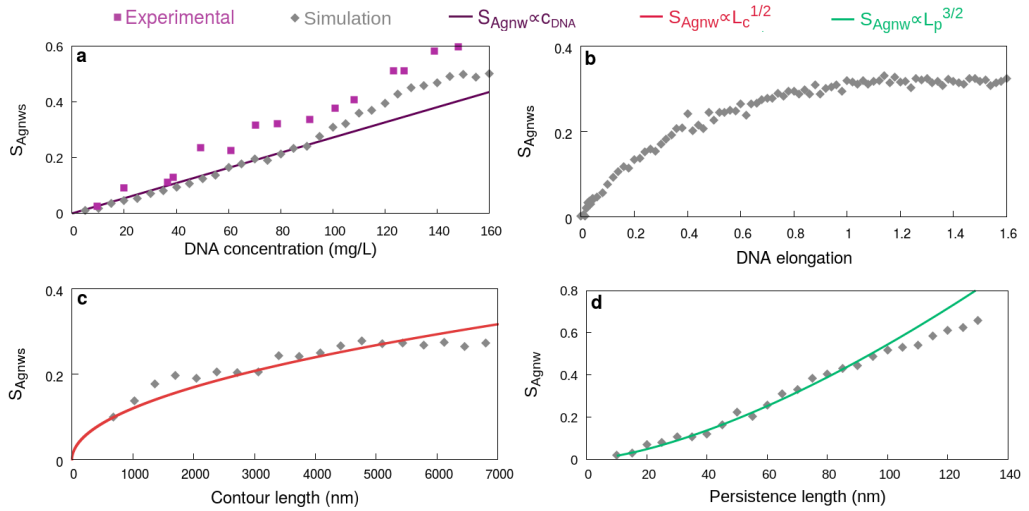

Figure 9: Simulation results of the orientational order parameter of the silver nanowires as a function of (a) DNA concentration, (b) coil elongation, (c) contour length of the chains, and (d) persistence length of the polymer. Unless indicated otherwise, c_{DNA}=100 mg/L, e=0.8, L_p=65 nm and L_c=5.1 μm. The grey points represent the simulation results. The coloured lines are fittings of these data to the $S_{\mathrm{Agnws}} \propto V_{\mathrm{ex}} \propto c_{\mathrm{DNA}}$, $S_{\mathrm{Agnws}} \propto V_{\mathrm{ex}} \propto L_c^{1/2}$ and $S_{\mathrm{Agnws}} \propto V_{\mathrm{ex}} \propto L_p^{3/2}$ dependencies. In (a), we also display the experimental results (coloured points) for comparison.

Fig. 9b shows the simulation results as a function of DNA elongation. The anomalous low-frequency effect grows with e, as expected, since Agnw orientation is induced by the anisotropy in the excluded volume. Indeed, it has been experimentally shown that the deformation of the DNA and the Agnw orientation at low frequencies are correlated: they both grow rapidly as the field frequency lowers, in a similar manner (Figs. 3 and 5). Our simulation qualitatively reproduces this correlation.

The results as a function of L_c are presented in Fig. 9c. As observed, our simulation predicts a more pronounced anomalous effect for larger values of the contour length, in agreement with the experimental results found for the PEO and the DNA with different molecular weights (Figs. 7a and 7b). The shape that our simulation predicts for this dependence can be qualitatively understood following the suggestion that $S_{\mathrm{Agnws}} \propto V_{\mathrm{ex}}$, which was already stated for the concentration dependence and supported by the experimental data. In the case of the contour length, $S_{\mathrm{Agnws}} \propto V_{\mathrm{ex}} \propto L_c^{1/2}$ (see SI file) [69]. As shown in the Figure, the simula-

tion data could indeed be suitably fitted to this dependence.

In Fig. 9d we display the order parameter given by the simulation for different values of L_p. As expected, the Agnw orientation grows with the persistence length, in line with the experimental results obtained for the PAA (Fig. 7c). In a similar manner to the previous case, the simulation data could be fitted to the $S_{\mathrm{Agnws}} \propto V_{\mathrm{ex}} \propto L_p^{3/2}$ dependence (see SI file).

4. Conclusions

In this work we have found that, under low frequency electric fields, DNA coils can induce a strong alignment on silver nanowires (Agnws) in suspension. This orientation is due solely to the presence of the DNA chains, and disappears completely for bare Agnw samples. Moreover, we experimentally show that this effect occurs also for Agnw-Poly(ethylene oxide), Agnw-Poly(acrylic acid) and sepiolite-DNA suspensions. Hence, the phenomenon is not exclusive of Agnws and DNA, but rather can be considered characteristic of particle-polymer systems.

Furthermore, we propose that this polymer-induced particle orientation occurring at low frequencies is due to anisotropic excluded volume interactions, which arise upon deformation of the polymer coils by the applied electric field. This hypothesis is supported by different experimental results, namely, the correlation between the Agnw orientation and the DNA stretching, the proportionality with the polymer concentration and the enhancement of the effect for longer and stiffer polymers. In addition, a computer simulation of the particle-polymer system has been presented, allowing to satisfactorily describe the experimental findings.

The controlled alignment of nanoparticles is a challenging topic, and necessary for many applications. Other approaches for polymer-mediated particle orientation are based either on polymer structures or a liquid crystalline phase [22, 54]. In the present investigation, polymer-induced orientation can be achieved using even dilute polymer solutions. We consider that this novel effect presents high prospects for particle orientation, since we have shown that it can be tuned by several parameters and that it occurs for particles and polymers of different nature. The phenomenon is most significant when DNA is used as the polymeric medium, since it is greatly enhanced by the persistence length.

Our results open up the possibility of exploring more complex systems. For instance, more concentrated polymer suspensions, well above the overlap concentration or even above the entanglement concentration, could lead to non-linearity or even to new behaviours. Polymer cross-linking may also have interesting effects and, for example, curing of the polymer could fix the alignment of the par-

ticles. The use of polymer mixtures, in which cooperative or antagonistic effects may arise, could also be considered.

Acknowledgement

Financial support of this investigation by *Junta de Andalucía*, Spain (*Programa operativo FEDER Andalucía 2014-2020*, Grant No. B-FQM-141-UGR18) and *Ministerio de Ciencia, Innovación y Universidades*, Spain (PGC2018-098770-B-I00) is gratefully acknowledged. P.A-G. thanks the University of Granada for her *contrato puente* (*Plan Propio*).

Appendix A. Supplementary material

Supplementary information to this article is provided as a single PDF file.

References

[1] E. Senses, S. Narayanan, Y. Mao, A. Faraone, Nanoscale particle motion in attractive polymer nanocomposites, Physical Review Letters 119(23) (2017) 237801.

[2] Gila-Vílchez, J. D. C., Durán, González-Caballero, A. F., Zubarev, M. T. López-López, Magnetorheology of alginate ferrogels, Smart Materials and Structures 28(3) (2019) 035018.

[3] L. W., L. Zhao, Z. Dai, H. Jin, F. Duan, J. Liu, Z. Zeng, J. Zhao, Z. Zhang, A temperature-activated nanocomposite metamaterial absorber with a wide tunability, Nano Research 11(7) (2018) 3931–3942.

[4] I. Pastoriza-Santos, C. Kinnear, J. Pérez-Juste, P. Mulvaney, L. M. Liz-Marzán, Plasmonic polymer nanocomposites, Nature Reviews Materials 3(10) (2018) 375–391.

[5] M. G. Kim, Y. Shon, W. Miao, J. Lee, Y. K. Oh, Biodegradable graphene oxide and polyaptamer DNA hybrid hydrogels for implantable drug delivery, Carbon 105 (2016) 14–22.

[6] Y. Liu, K. Zhang, W. Li, J. Ma, G. J. Vancso, Metal nanoparticle loading of gel-brush grafted polymer fibers in membranes for catalysis, Journal of Materials Chemistry A 6(17) (2018) 7741–7748.

[7] B. Xie, H. Zhang, Q. Zhang, Z. Jiadong, C. Yang, Q. Wang, M. Li, S. Jiang, Enhanced energy density of polymer nanocomposites at a low electric field through aligned $BaTiO_3$ nanowires, Journal of Materials Chemistry A 5(13) (2017) 6070–6078.

[8] J. Li, Q. Zhou, C. Yuan, P. Cheng, X. Hu, W. Huang, X. Gao, X. Wang, M. Jin, R. Nötzel, G. Zhou, Z. Zhang, J. Liu, Direct growth of vertically aligned $ReSe_2$ nanosheets on conductive electrode for electro-catalytic hydrogen production, Journal of Colloid and Interface Science 553 (2019) 699–704.

[9] M. Sun, B. Dai, K. Liu, K. Yao, J. Zhao, Z. Lyu, P. Wang, Y. Ding, L. Yang, J. Han, J. Zhu, Enhancement in thermal conductivity of polymer composites using aligned diamonds coated with superparamagnetic magnetite, Composites Science and Technology 164 (2018) 129–135.

[10] T. Zhang, J. Sun, L. Ren, Y. Yao, M. Wang, X. Zeng, R. Sun, J. B. Xu, C. P. Wong, Nacre-inspired polymer composites with high thermal conductivity and enhanced mechanical strength, Composites Part A: Applied Science and Manufacturing 121 (2019) 92–99.

[11] J. Hu, Y. Huang, X. Zeng, Q. Li, L. Ren, R. Sun, J. B. Xu, C. P. Wong, Polymer composite with enhanced thermal conductivity and mechanical strength through orientation manipulating of BN, Composites Science and Technology 160 (2018) 127–137.

[12] Z. Liu, P. Peng, Z. Liu, W. Fang, Q. Zhou, X. Liu, J. Liu, Electric-field-induced out-of-plane alignment of clay in poly (dimethylsiloxane) with enhanced anisotropic thermal conductivity and mechanical properties, Composites Science and Technology 165 (2018) 39–47.

[13] C. Baratto, V. Golovanova, G. Faglia, H. Hakola, T. Niemi, N. Tkachenko, B. Nazarchurk, V. Golovanov, On the alignment of ZnO nanowires by Langmuir–Blodgett technique for sensing application, Applied Surface Science (2020) 146959.

[14] G. Xin, W. Zhu, Y. Deng, J. Cheng, L. T. Zhang, A. J. Chung, S. De, J. Lian, Microfluidics-enabled orientation and microstructure control of macroscopic graphene fibres, Nature Nanotechnology 14(2) (2019) 168–175.

[15] D. Kumar, A. Shenoy, S. Li, C. M. Schroeder, Orientation control and nonlinear trajectory tracking of colloidal particles using microfluidics, Physical Review Fluids 4(11) (2019) 114203.

[16] H. Sakamoto, I. Fujiwara, E. Takamura, S. I. Suye, Nanofiber-guided orientation of electrospun carbon nanotubes and fabrication of aligned CNT electrodes for biodevice applications, Materials Chemistry and Physics 245 (2020) 122745.

[17] W. Ning, Z. Wang, P. Liu, D. Zhou, Y. S., J. Wang, Q. Li, S. Fan, K. Jiang, Multifunctional super-aligned carbon nanotube/polyimide composite film heaters and actuators, Carbon 139 (2018) 1136–1143.

[18] L. Li, T. Yang, K. Wang, H. Fan, C. Hou, Q. Zhang, Y. Li, H. Yu, H. Wang, Mechanical design of brush coating technology for the alignmentof one-dimension nanomaterials, Journal of Colloid and Interface Science 583 (2021) 188–195.

[19] H. Hu, M. Pauly, O. Felix, G. Decher, Spray-assisted alignment of Layer-by-Layer assembled silver nanowires: a general approach for the preparation of highly anisotropic nano-composite films, Nanoscale 9(3) (2017) 1307–1314.

[20] H. Zhang, D. Fu, Z. Du, H. Fu, G. Shao, W. Yang, J. Zheng, In situ growth of aligned $CsPbBr_3$ nanorods in polymer fibers with tailored aspect ratios, Ceramics International 46(11) (2020) 18352–18357.

[21] P. Mardle, X. Ji, J. Wu, S. Guan, H. Dong, S. Du, Thin film electrodes from Pt nanorods supported on aligned N-CNTs for proton exchange membrane fuel cells, Applied Catalysis B: Environmental 260 (2020) 118031.

[22] Q. Liu, J. S. Campbell, M. G. an Evans, I. I. Smalyukh, Orientationally ordered colloidal co-dispersions of gold nanorods and cellulose nanocrystals, Advanced Materials 26(42) (2014) 7178–7184.

[23] D. L. Fan, F. Q. Zhu, R. C. Cammarata, C. L. Chien, Controllable high-speed rotation of nanowires, Physical Review Letters 94(24) (2005) 247208.

[24] F. Lin, Z. Zhu, X. Zhou, W. Qiu, C. Niu, J. Hu, K. Dahal, Y. Wang, Z. Zhao, Z. Ren, D. Litvinov, Z. Liu, Z. M. Wang, J. Bao, Orientation control of graphene flakes by magnetic field: broad device applications of macroscopically aligned graphene, Advanced Materials 29(1) (2017) 1604453.

[25] Y. He, S. Yang, H. Liu, Q. Shao, Q. Chen, C. Lu, Y. Jiang, C. Liu, Z. Guo, Reinforced carbon fiber laminates with oriented carbon nanotube epoxy nanocomposites: magnetic field assisted alignment and cryogenic temperature mechanical properties, Journal of Colloid and Interface Science 517 (2018) 40–51.

[26] Arenas-Guerrero, M. L. P., Jiménez, K. Scott, K. J. Donovan, Electric birefringence of carbon nanotubes: Single-vs double-walled, Carbon 126 (2018) 77–84.

[27] D. Matsunaga, F. Meng, Z. A., R. Golestanian, J. M. Yeomans, Focusing and sorting of ellipsoidal magnetic particles in microchannels, Physical Review Letters 119(19) (2017) 198002.

[28] A. I. Oliva-Avilés, F. Avilés, V. Sosa, Electrical and piezoresistive properties of multi-walled carbon nanotube/polymer composite films aligned by an electric field, Carbon 49(9) (2011) 2989–2997.

[29] S. Yun, T. Guo, Y. Li, X. Gao, A. Huang, L. Kang, Well-ordered vertically aligned ZnO nanorods arrays for high-performance perovskite solar cells, Materials Research Bulletin 130 (2020) 110935.

[30] J. Oh, M. Y. Ryu, Structural and optical properties of the perovskite layer on well-aligned ZnO nanorods, Applied Science and Convergence Technology 29(4) (2020) 91–93.

[31] S. Kaur, G. Murali, R. Manda, Y. C. Chae, M. Yun, J. H. Lee, S. H. Lee, Functional film with electric-field-aided aligned assembly of quantum rods for potential application in liquid crystal display, Advanced Optical Materials 6(17) (2018) 1800235.

[32] S. K. Gupta, M. F. Prodanov, W. Zhang, V. V. Vashchenko, T. Dudka, A. L. Rogach, A. K. Srivastava, Inkjet-printed aligned quantum rod enhancement films for their application in liquid crystal displays, Nanoscale 11(43) (2019) 20837–20846.

[33] W. Wei, Y. Wang, J. Ji, S. Zuo, W. Li, F. Bai, H. Fan, Fabrication of large-area arrays of vertically aligned gold nanorods, Nano Letters 18(7) (2018) 4467–4472.

[34] A. Apte, P. Joshi, P. Bhaskar, D. Joag, S. Kulkarni, Vertically aligned self-assembled gold nanorods as low turn-on, stable field emitters, Applied Surface Science 355 (2015) 978–983.

[35] M. Mazaheri, A. Simchi, H. Aashuri, Enzymatic biosensing by covalent conjugation of enzymes to 3D-networks of graphene nanosheets on arrays of vertically aligned gold nanorods: Application to voltammetric glucose sensing, Microchimica Acta 185(3) (2018) 178.

[36] H. Zhang, Y. Liu, M. F. S. Shahidan, C. Kinnear, F. Maasoumi, J. Cadusch, A. E. M., T. D. James, A. Widmer-Cooper, A. Roberts, P. Mulvaney, Direct assembly of vertically oriented, gold nanorod arrays, Advanced Functional Materials (2020) 2006753.

[37] T. Fukagawa, H. Tanaka, K. Morikawa, S. Tanaka, Y. Hatakeyama, K. Hino, Spatial ordering of the structure of polymer-capped gold nanorods under an external DC electric field, The Journal of Physical Chemistry Letters 11(6) (2020) 2086–2091.

[38] S. Etcheverry, L. F. Araujo, G. K. B. da Costa, J. M. B. Pereira, A. R. Camara, J. Naciri, B. R. Ratna, I. Hernández-Romano, C. J. S. de Matos, I. C. S. Carvalho, W. Margulis, J. Fontana, Microsecond switching of plasmonic nanorods in an all-fiber optofluidic component, Optica 4(8) (2017) 864–870.

[39] P. Arenas-Guerrero, Á. V. Delgado, A. Ramos, M. L. Jiménez, Electro-orientation of silver nanowires in alternating fields, Langmuir 35(3) (2018) 687–694.

[40] P. Arenas-Guerrero, S. Ahualli, Á. V. Delgado, M. L. Jiménez, Birefringence of gold nanorods: effect of surfactant coating, The Journal of Physical Chemistry C 123(43) (2019) 26623–26632.

[41] J. W. Liaw, W. J. Lo, W. C. Lin, M. K. Kuo, Theoretical study of optical torques for aligning Ag nanorods and nanowires, Journal of Quantitative Spectroscopy and Radiative Transfer 162 (2015) 133–142.

[42] F. Xu, W. Xu, B. Mao, W. Shen, Y. Yu, R. Tan, W. Song, Preparation and cold welding of silver nanowire based transparent electrodes with optical transmittances $>$90% and sheet resistances $<$10 ohm/sq, Journal of Colloid and Interface Science 512 (2018) 208–218.

[43] T. Wang, C. Luo, F. Liu, L. Li, Y. Zhang, X.and Li, E. H. Han, Y. Fu, Y. Jiao, Highly transparent, conductive, and bendable Ag nanowire electrodes with enhanced mechanical stability based on polyelectrolyte adhesive layer, Langmuir 33(19) (2017) 4702–4708.

[44] Z. Yu, L. Li, Q. Zhang, W. Hu, Q. Pei, Silver nanowire-polymer composite electrodes for efficient polymer solar cells, Advanced Materials 23(38) (2011) 4453–4457.

[45] C. Gong, J. Liang, W. Hu, X. Niu, S. Ma, H. T. Hahn, Q. Pei, A healable, semitransparent silver nanowire-polymer composite conductor, Advanced Materials 25(30) (2013) 4186–4191.

[46] S. Cho, S. Kang, A. Pandya, R. Shanker, Z. Khan, Y. Lee, J. Park, S. Craig, H. Ko, Large-area cross-aligned silver nanowire electrodes for flexible, transparent, and force-sensitive mechanochromic touch screens, ACS Nano 11(4) (2017) 4346–4357.

[47] F. Wu, Z. Li, F. Ye, X. Zhao, T. Zhang, X. Yang, Aligned silver nanowires as transparent conductive electrodes for flexible optoelectronic devices, Journal of Materials Chemistry C 4(47) (2016) 11074–11080.

[48] S. Kang, T. Kim, S. Cho, Y. Lee, A. Choe, B. Walker, S. J. Ko, J. Y. Kim, H. Ko, Capillary printing of highly aligned silver nanowire transparent electrodes for high-performance optoelectronic devices, Nano Letters 15(12) (2015) 7933–7942.

[49] Y. Chen, W. Lan, J. Wang, R. Zhu, Z. Yang, D. Ding, G. Tang, K. Wang, Q. Su, E. Xie, Highly flexible, transparent, conductive and antibacterial films made of spin-coated silver nanowires and a protective ZnO layer, Physica E: Low-Dimensional Systems and Nanostructures 76 (2016) 88–94.

[50] Q. Zhang, Y. Qiao, F. Hao, L. Zhang, S. Wu, Y. Li, J. Li, X. M. Song, Fabrication of a biocompatible and conductive platform based on a single-stranded DNA/graphene nanocomposite for direct electrochemistry and electrocatalysis, Chemistry-A European Journal 16(27) (2010) 8133–8139.

[51] T. Premkumar, K. E. Geckeler, Graphene–DNA hybrid materials: Assembly, applications, and prospects, Progress in Polymer Science 37(4) (2012) 515–529.

[52] H. Garmestani, M. S. Al-Haik, K. Dahmen, R. Tannenbaum, D. Li, S. S. Sablin, M. Y. Hussaini, Polymer-mediated alignment of carbon nanotubes under high magnetic fields, Advanced Materials 15(22) (2011) 1918–1921.

[53] J. Pérez-Juste, B. Rodríguez-González, P. Mulvaney, L. M. Liz-Marzán, Optical control and patterning of gold-nanorod–poly (vinyl alcohol) nanocomposite films, Advanced Functional Materials 15(7) (2005) 1065–1071.

[54] Y. J. Cha, D. S. Kim, D. K. Yoon, Highly aligned plasmonic gold nanorods in a DNA matrix, Advanced Functional Materials 27(45) (2017) 1703790.

[55] P. Arenas-Guerrero, Á. V. Delgado, K. J. Donovan, K. Scott, T. Bellini, F. Mantegazza, M. L. Jiménez, Determination of the size distribution of non-spherical nanoparticles by electric birefringence-based methods, Scientific Reports 8(1) (2018) 1–10.

[56] A. W. Schell, A. Kuhlicke, G. Kewes, O. Benson, "flying plasmons": Fabry-Pèrot resonances in levitated silver nanowires, ACS Photonics 4(11) (2017) 2719–2725.

[57] C. T. O'Konski, Molecular Electro-Optics, Marcel Dekker, 1976.

[58] J. J. Arcenegui, P. García-Sánchez, H. Morgan, A. Ramos, Electro-orientation and electrorotation of metal nanowires, Physical Review E 88(6) (2013) 063018.

[59] R. S. Wilkinson, G. B. Thurston, The optical birefringence of DNA solutions induced by oscillatory electric and hydrodynamic fields, Biopolymers: Original Research on Biomolecules 15(8) (1976) 1555–1572.

[60] M. Washizu, O. Kurosawa, Electrostatic manipulation of DNA in microfabricated structures, IEEE Transactions on Industry Applications 26(6) (1990) 1165–1172.

[61] J. M. Kim, T. Ohtani, J. Y. Park, S. M. Chang, H. Muramatsu, DC electric-field-induced DNA stretching for AFM and SNOM studies, Ultramicroscopy 91(1-4) (2002) 139–149.

[62] M. Ueda, H. Iwasaki, O. Kurosawa, M. Washizu, Atomic force microscopy observation of deoxyribonucleic acid stretched and anchored onto aluminum electrodes, Japanese Journal of Applied Physics 38(4R) (1999) 2118.

[63] Y. Wang, M. Gao, Y. Qu, J. Hu, Y. Xie, Z. Liu, Z. Song, H. Xu, Z. Weng, Z. Wang, Effects of AC/DC electric fields on stretching DNA molecules, NANO 15(5) (2020) 2050065.

[64] N. C. Stellwagen, Electric birefringence of restriction enzyme fragments of DNA: optical factor and electric polarizability as a function of molecular weight, Biopolymers: Original Research on Biomolecules 20(3) (1981) 399–434.

[65] M. F. Maestre, R. Kilkson, Intrinsic birefringence of multiple-coiled DNA, theory and applications, Biophysical journal 5(3) (1965) 275–287.

[66] Q. Liu, M. Li, Y. Gu, Y. Zhang, S. Wang, Q. Li, Z. Zhang, Highly aligned dense carbon nanotube sheets induced by multiple stretching and pressing, Nanoscale 6(8) (2014) 4338–4344.

[67] D. Jia, M. Muthukumar, Topologically frustrated dynamics of crowded charged macromolecules in charged hydrogels, Nature Communications 9(1) (2018) 1–12.

[68] K. Tanaka, Y. Okahata, A DNA-lipid complex in organic media and formation of an aligned cast film, Journal of the American Chemical Society 118(44) (1996) 10679–10683.

[69] I. Teraoka, Polymer Solutions, John Wiley & Sons, Inc, 2002.

[70] G. C. Patel, P. V. K., P. S. Patel, Stimuli-responsive polymers for ocular therapy, in: A. S. H. Makhlouf, N. Y. Abu-Thabit (Eds.), Stimuli Responsive Polymeric Nanocarriers for Drug Delivery Applications: Volume 2, Woodhead Publishing, 2019, Ch. 17, pp. 433–452.

[71] P. J. Hagerman, Investigation of the flexibility of DNA using transient electric birefringence, Biopolymers: Original Research on Biomolecules 20(7) (1934) 1503–1535.

[72] C. N. Likos, N. Hoffmann, H. Löwen, A. A. Louis, Exotic fluids and crystals of soft polymeric colloids, Journal of Physics: Condensed Matter 14(33) (2002) 7681.